SUPPLEMETARY DATA

Hepatic GSK3β-dependent CRY1 Degradation Contributes to Diabetic Hyperglycemia

Ye Young Kim, Hagoon Jang, Gung Lee, Yong Geun Jeon, Jee Hyung Sohn, Ji Seul Han, Won Taek Lee, Jeu Park, Jin Young Huh, Hahn Nahmgoong, Sang Mun Han, Jeesoo Kim, Minwoo Pak, Sun Kim, Jong-Seo Kim, and Jae Bum Kim

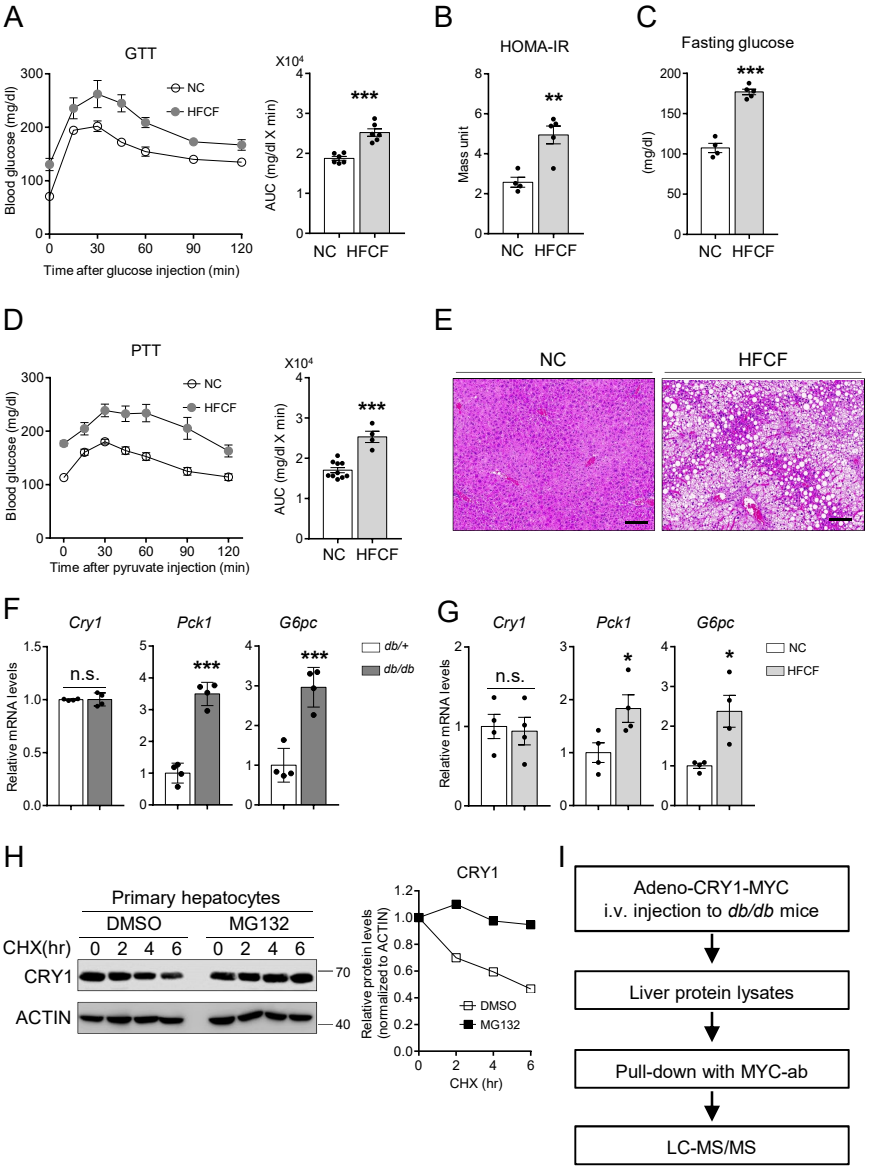

Supplementary Figure 1. The phenotype of NC-fed and HFCF-fed mice and strategy of CRY1 binding proteins in the liver. A: Intraperitoneal GTT and AUC analysis of NC- or HFCF-fed WT mice. ***$P < 0.001$ vs. NC-fed WT mice by Student's *t*-test. B and C: Measurement of HOMA-IR (B) and fasting blood glucose levels (C) of NC- or HFCF-fed WT mice. **$P < 0.01$, ***$P < 0.001$ vs. NC-fed WT mice by Student's *t*-test. D: Intraperitoneal PTT and AUC analysis of NC- or HFCF-fed WT mice. ***$P < 0.001$ vs. NC-fed WT mice by Student's *t*-test. E: Representative images of hematoxylin and eosin-stained sections of livers of NC- or HFCF-fed WT mice. F and G: qRT-PCR analyses of *Cry1* and gluconeogenic gene (*Pck1* and *G6pc*) expression in liver lysates from *db/+* and *db/db* mice (F) and NC- and HFCF-fed mice (G). *$P < 0.05$, ***$P < 0.001$ vs. each control group by Student's *t*-test. H: CRY1 protein stability in primary hepatocytes treated with CHX (30 μmol/L) for the indicated periods with or without MG132 (20 μmol/L) treatment. I: Experimental strategy of the LC-MS/MS analysis to identify CRY1 binding proteins in the liver. Mean and SEM of the band intensities were calculated from independent experiments using Image J. Data are mean ±SEM. n.s., not significant; CHX, cycloheximide.

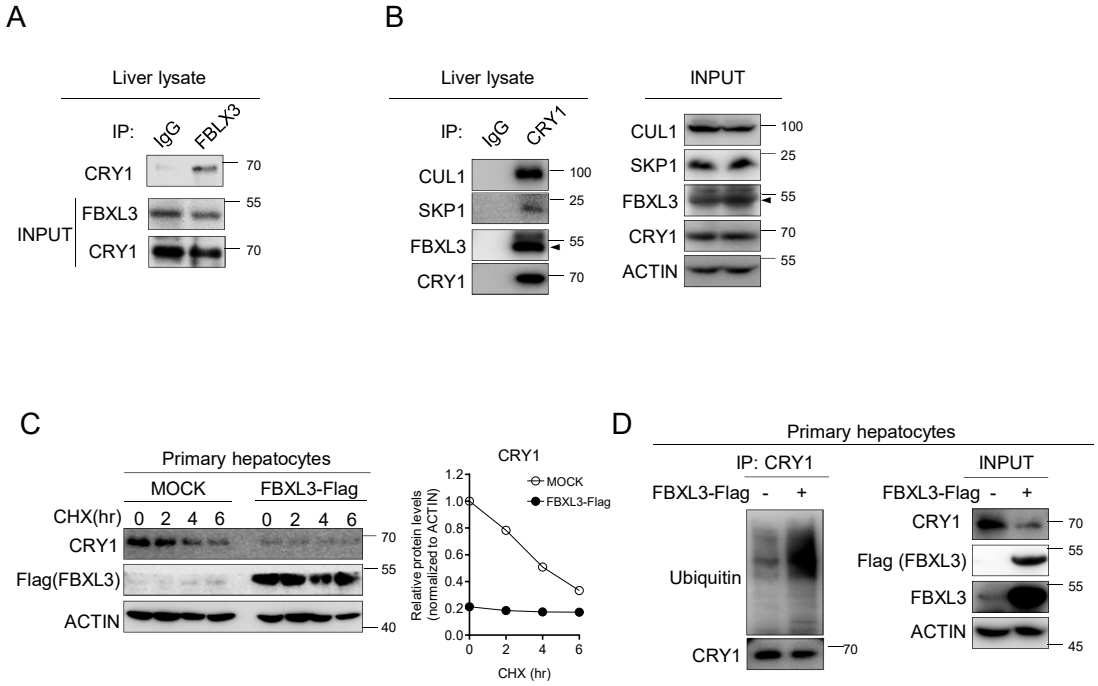

Supplementary Figure 2. FBXL3 regulates CRY1 protein stability in hepatocytes. A: Endogenous coimmunoprecipitation using FBXL3 antibody with liver lysates. B: Endogenous coimmunoprecipitation using CRY1 antibody with liver lysates. C: CRY1 protein stability. Primary hepatocytes were transfected with MOCK or FBXL3 expression vectors and were harvested at the indicated time points after CHX (30 μmol/L) treatment. D: Cell-based ubiquitination assay in primary hepatocytes. Cells were transfected with MOCK or FBXL3 expression vectors without MG132 treatment. Mean and SD of the band intensities were calculated from independent experiments using Image J. Data are mean ±SD.

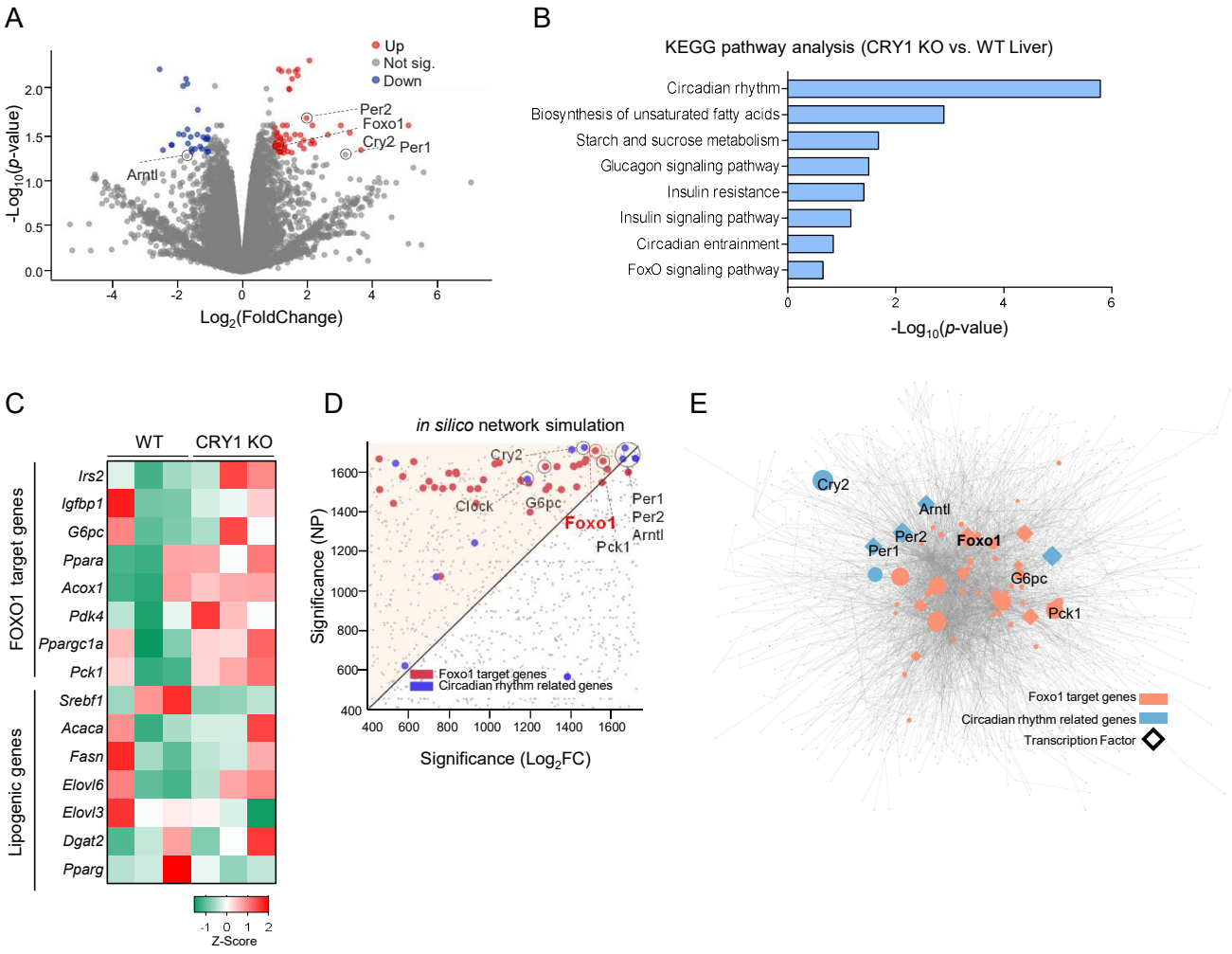

Supplementary Figure 3. FOXO1 target genes are highly expressed in liver of CRY1 KO mice. A: Volcano plot of differentially expressed genes (DEG) identified with 0.05 > *adjusted p-value* threshold. Red dots represent upregulated genes and blue dots represent downregulated genes of the plot. B: KEGG pathway enrichment of upregulated genes in liver from CRY1 KO. C: Heatmap showing the expression levels of FOXO1 target genes and lipogenic genes in liver from CRY1 KO and WT mice. D: Scatter plot representing gene significance of network propagation (NP) scores and fold change (FC). Red dots represent genes that are FOXO1 target genes and blue dots represent circadian rhythm-related genes. E: The whole transcription-factor target gene (TFTG) network containing genes in the FOXO1 target genes and circadian rhythm-related genes, respectively. Node size corresponds to NP score. The higher the NP score, the bigger the node size.

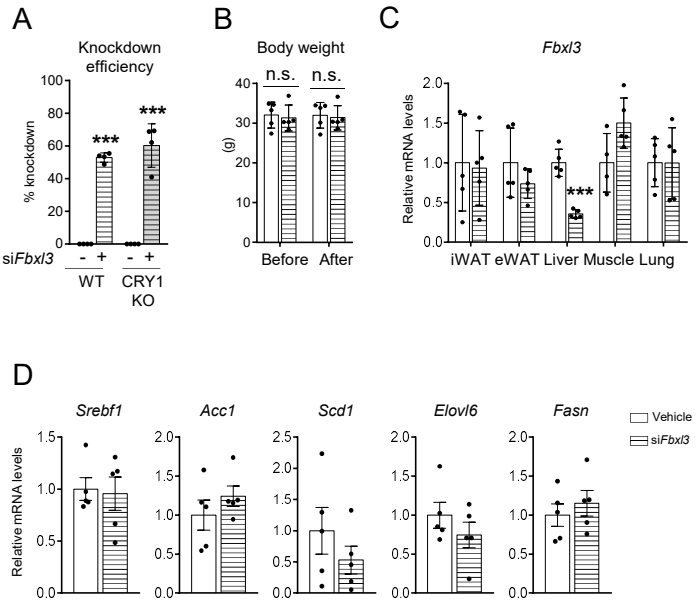

Supplementary Figure 4. FBXL3-CRY1 axis regulates hepatic glucose production. A: Knockdown efficiency of *Fbxl3* gene expression in primary hepatocytes from WT and CRY1 KO. ***P < 0.001 vs. WT, siNC group by two-way ANOVA followed by Sidak's post-hoc test. B: Body weights of vehicle-treated and si*Fbxl3*-treated mice before and after treatment. C: qRT-PCR analysis of *Fbxl3* in inguinal white adipose tissue (iWAT), epididymal white adipose tissue (eWAT), liver, skeletal muscle, and lung of vehicle-treated and si*Fbxl3*-treated mice. D: qRT-PCR analysis of lipogenic gene expression in liver of vehicle-treated and si*Fbxl3*-treated mice.

A

Phosphorylation site	Sequence	Predicted kinase
CRY1 S71	NLRKLN**s**RLFVIR	AMPK
CRY1 S247	ANSLLA**s**PTGLSP	MAPK
CRY1 S281	KVKKNS**s**PPLSLY	GSK3β
CRY1 S588	SSGKRP**s**QEEDAQ	DNA-PK
CRY1 S595	QEEDAQ**s**VGPKVR	CK-1

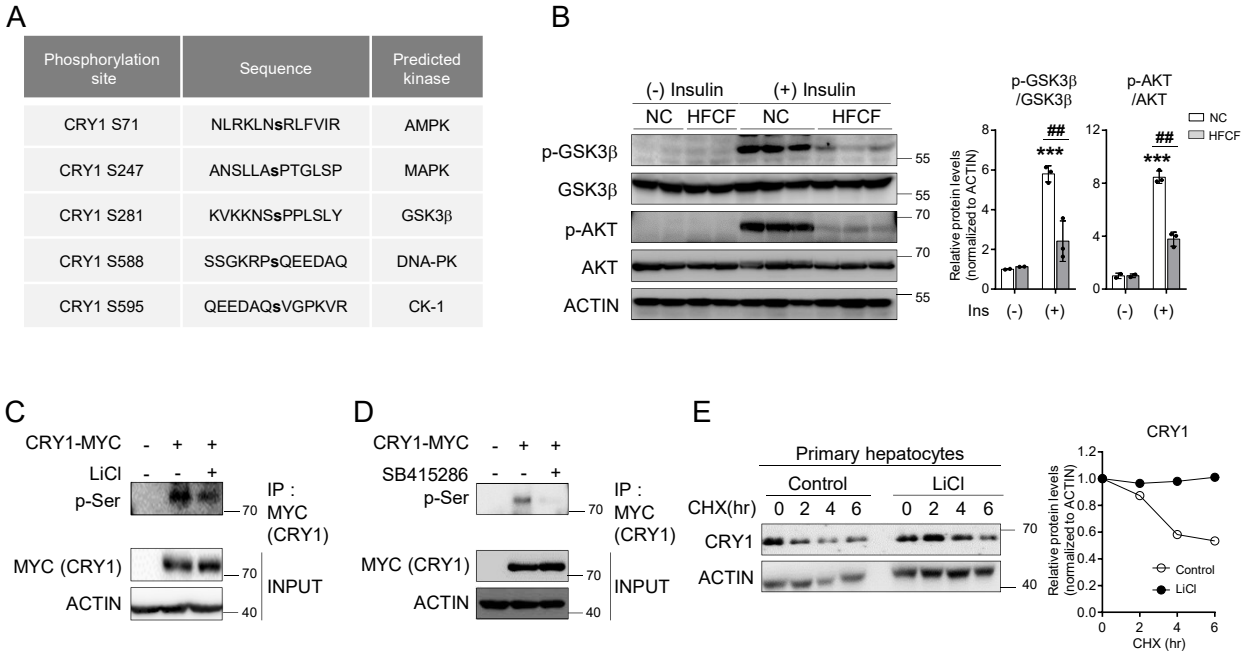

Supplementary Figure 5. GSK3β is involved in CRY1 phosphorylation and FBXL3-dependent degradation. A: Scansite 4.0 and phosphoSitePlus predictions of mouse CRY1 phosphorylation sites [37, 38]. B: Western blot analysis of insulin signaling cascade in liver lysates from NC- or HFCF-fed mice. ***$P < 0.001$ vs. vehicle-treated NC-fed WT mice; ##$P < 0.01$ vs. vehicle-treated HFCF-fed WT mice by two-way ANOVA followed by Sidak's post-hoc test. C and D: Immunoprecipitation-western blot analysis of the level of CRY1 protein phosphorylation in HEK293T cells treated without or with GSK3β inhibitor LiCl (20 mmol/L) (C) or SB415286 (20 μmol/L) (D) for 2 h. E: CRY1 protein stability in primary hepatocytes treated with CHX (30 μmol/L) for the indicated periods with or without GSK3β inhibitor LiCl (20 mmol/L). F: Cell-based ubiquitination assay. COS1 cells were cotransfected without or with plasmids encoding CRY1-MYC, ubiquitin-HA, and FBXL3-Flag. Cells were incubated without or with LiCl (20 mmol/L) prior to MG132 (20 μmol/L) treatment for 6 h. Mean and SD of the band intensities were calculated from independent experiments using Image J. Data are mean ±SD. UB, ubiquitin; CHX, cycloheximide; IP, immunoprecipitation.

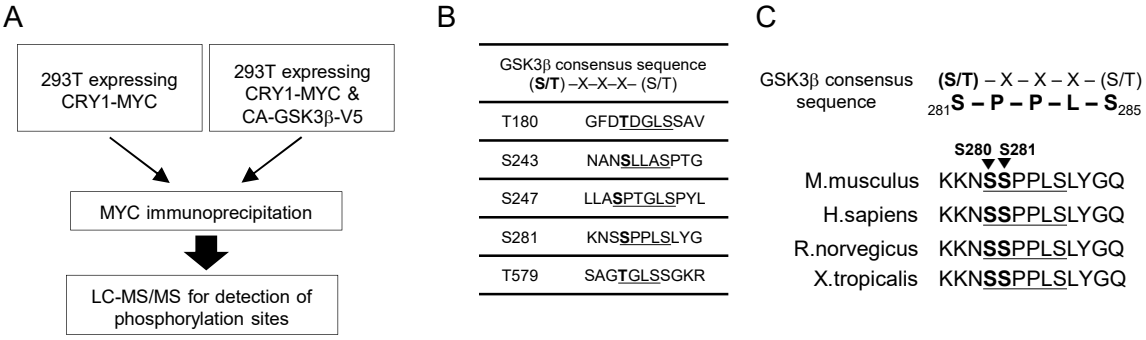

Supplementary Figure 6. MS-based and *in silico* analyses of potential phosphorylation residue(s) in the CRY1 protein by GSK3β. A: Scheme of MS analysis to identify CRY1 phosphorylation sites using liver lysates of *db/db* mice. B: Identification of GSK3β phosphorylation sites in CRY1 (data from GPS 5.0 software (http://gps.biocuckoo.cn) [37]). C: Alignment of CRY1 amino acid sequences from several species with potential CRY1 phosphorylation sites.

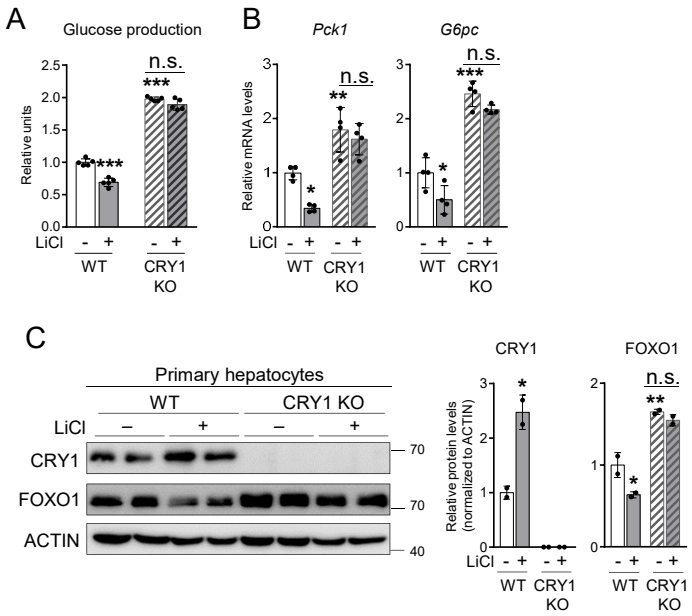

Supplementary Figure 7. Inhibition of GSK3β downregulates CRY1-mediated gluconeogenesis in hepatocytes. A–C: Primary hepatocytes isolated from WT and CRY1 KO mice were incubated without or with LiCl (20 mmol/L) for 8 h. Glucose production assay (A), qRT-PCR analysis of gluconeogenic gene expression (B), and western blot analysis of CRY1 and FOXO1 protein (C) are shown. *P < 0.05, **P < 0.01, ***P < 0.001 vs. WT, PBS group by two-way ANOVA followed by Sidak's post-hoc test. Mean and SD of the band intensities were calculated from independent experiments using Image J. Data are mean ±SD.

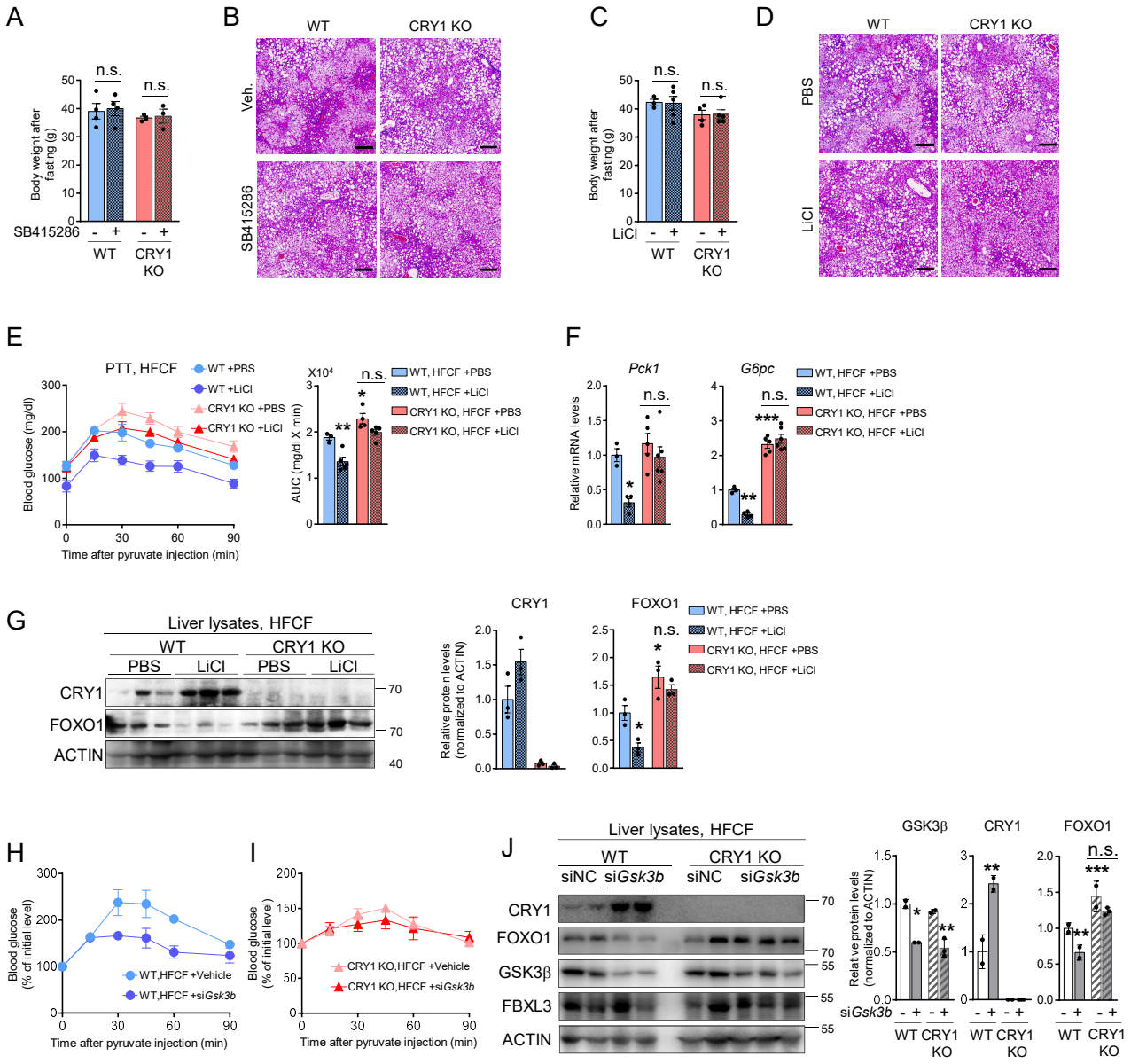

Supplementary Figure 8. GSK3β suppression restores CRY1 protein and alleviates HGP. A–B: SB415286 (5 mg/kg) was intraperitoneally injected into HFCF-fed WT or CRY1 KO mice. Body weights (A), representative images of hematoxylin and eosin-stained liver sections (B) of vehicle or SB415286-treated mice. C–G: LiCl (3 mM/kg) was intraperitoneally injected into HFCF-fed WT or CRY1 KO mice. Body weights (C), representative images of hematoxylin and eosin-stained liver sections (D), Intraperitoneal PTT and AUC analysis (E) of vehicle or LiCl-treated mice. qRT-PCR analysis of gluconeogenic gene expression (F) and western blot analysis (G) in the livers of vehicle or LiCl-treated mice. *$P < 0.05$, *$P < 0.01$, ***$P < 0.001$ vs. vehicle-treated HFCF-fed WT mice by two-way ANOVA followed by Sidak's post-hoc test. H–J: si*Gsk3b* was intravenously injected into HFCF-fed WT or CRY1 KO mice. Intraperitoneal PTT analysis of HFCF-fed WT mice (H), Intraperitoneal PTT analysis of HFCF-fed CRY1 KO mice (I). Western blot analysis of livers of HFCF-fed WT and KO mice (J). Mean and SEM of the band intensities were calculated from independent experiments using Image J. Data are mean ±SEM. n.s., not significant.

Supplementary Table 1. List of the putative binding proteins of CRY1.

Proteins	Full names
PER1	Period circadian clock 1
FBXL3	F-box and leucine-rich repeat protein 3
SKP1	S-phase kinase-associated protein 1
DTX3L	Deltex 3-like, E3 ubiquitin ligase
TLK2	Serine/threonine-protein kinase tousled-like 2
FASN	Fatty acid synthase
Timm9	Translocase of inner mitochondrial membrane 9
PYC	Pyruvate carboxylase, mitochondrial
RL40	Ubiquitin-60S ribosomal protein L40
THIKB	3-ketoacyl-CoA thiolase B, peroxisomal
APOE	Apolipoprotein E
ECHM	Enoyl-CoA hydratase, mitochondrial
AATM	Aspartate aminotransferase, mitochondrial
GPX1	Glutathione peroxidase 1
PLIN4	Perilipin-4
ACADV	Very long-chain specific acyl-CoA dehydrogenase, mitochondrial
CX6B1	Cytochrome c oxidase subunit 6B1
THIM	3-ketoacyl-CoA thiolase, mitochondrial
AL1L1	Cytosolic 10-formyltetrahydrofolate dehydrogenase
ODPB	Pyruvate dehydrogenase E1 component subunit beta, mitochondrial
APOA1	Apolipoprotein A-I
NDUA7	NADH dehydrogenase [ubiquinone] 1 alpha subcomplex subunit 7
ACLY	ATP-citrate synthase

Supplementary Table 2. Primers used for qRT-PCR

Gene	Forward	Reverse
Mouse Cry1	GTGGATCAGCTGGGAAGAAG	CACAGGGCAGTAGCAGTGAA
Mouse Fbxl3	CAGGACTCTGCTGAGGAAGG	CAGCTGATTCTTTGCTGCTG
Mouse Pck1	ATCTTTGGTGGCCGTAGACCT	CCGAAGTTGTAGCCGAAGAA
Mouse G6pc	AGGAAGGATGGAGGAAGGAA	TGGAACCAGATGGGAAAGAG
Mouse Dtx3l	GAATGCAGCCTTACCTGCTC	TGGCTTTGCTGATACACGAG
Mouse Tbp	GGGAGAATCATGGACCAGAA	CCGTAAGGCATCATTGGACT

Supplementary Table 3. NP score of candidate genes in liver of CRY1 KO mice compared to WT

Proteins	NP_score	Log2FC	NP_score_rank	Log2FC_rank	NP_rank_ratio
Cyp3a11	0.2188	1.6401	1	97	0.0578
Bik	0.2147	0.4220	2	619	0.1157
Cpt1a	0.2142	0.7082	3	349	0.1735
Nfe2l2	0.2114	0.6373	4	390	0.2313
Bhlhe40	0.2103	1.8925	5	74	0.2892
Cry2	0.2056	0.8738	6	264	0.3470
Per2	0.2055	1.9774	7	65	0.4049
Pklr	0.2054	0.7348	8	328	0.4627
Dbp	0.2050	2.2127	9	53	0.5205
Skil	0.2037	-0.7206	10	335	0.5784
Txnip	0.2037	2.1550	11	57	0.6362
Scd1	0.2015	1.2493	12	157	0.6940
Elovl5	0.2015	0.9301	13	240	0.7519
Zbtb16	0.2009	3.3035	14	13	0.8097
Gys2	0.2009	0.8967	15	257	0.8676
Hnf4a	0.2007	0.7358	16	326	0.9254
Tfb2m	0.2006	0.4572	17	563	0.9832
Il6ra	0.2005	2.1051	18	60	1.0411
Pex11a	0.2004	0.7733	19	307	1.0989
Lgals4	0.2004	1.4320	19	131	1.0989
Tert	0.2004	-0.9635	21	232	1.2146
Foxo1	0.2002	1.0077	22	212	1.2724
Itga7	0.2002	-0.7295	23	332	1.3302
Bnip3	0.2002	0.7803	24	302	1.3881
Wee1	0.2001	3.0286	25	21	1.4459
Krt18	0.2001	-0.7112	25	346	1.4459
Mmp15	0.2001	0.5431	27	464	1.5616
Glrx	0.2000	-0.9197	28	247	1.6194
Rorc	0.2000	1.4534	29	128	1.6773
Hinfp	0.2000	1.1789	30	167	1.7351
Slc20a1	0.2000	1.3023	31	147	1.7929
Zbtb20	0.2000	1.0042	32	214	1.8508
Tgm1	0.2000	-1.5686	33	111	1.9086
Pdk1	0.2000	1.0045	34	213	1.9665
St3gal5	0.2000	1.8960	35	72	2.0243
Nfyb	0.2000	-0.7379	36	325	2.0821
Rgs16	0.2000	5.1011	37	3	2.1400
Sh3bp2	0.2000	-0.5651	38	451	2.1978
Stard5	0.2000	0.5030	39	512	2.2556
Herpud1	0.2000	1.7795	39	84	2.2556
Klf10	0.2000	2.6314	41	33	2.3713
Nr1i3	0.2000	1.3975	41	134	2.3713
Klf13	0.2000	1.2988	41	149	2.3713
Hlf	0.2000	1.1858	41	166	2.3713
Tef	0.2000	1.5343	41	115	2.3713
Nr1d2	0.2000	0.8665	41	268	2.3713
Atf4	0.2000	-0.5334	41	479	2.3713
Sall1	0.2000	0.9648	41	230	2.3713
Trim24	0.2000	0.7176	41	337	2.3713
Il2ra	0.1698	-0.3575	50	704	2.8918
Gja1	0.1616	0.6764	51	363	2.9497
Sox9	0.1605	0.8760	52	263	3.0075
Ccl5	0.1604	-0.5540	53	459	3.0654
Stat1	0.1600	-0.5304	54	482	3.1232
Abcb1a	0.1600	0.3311	55	755	3.1810
Kif26b	0.1600	0.2025	56	1033	3.2389
Cdkn1a	0.1196	0.1022	57	1373	3.2967
Ddit4	0.0806	1.0766	58	191	3.3545
Ctnnb1	0.0697	0.0322	59	1627	3.4124
Per1	0.0597	3.1719	60	15	3.4702

Supplementary Table 4. MS/MS data of the putative binding proteins of CRY1, related to Fig. 1C.